ACS NANO
Cite This: ACS Nano 2017, 11, 9898-9905
www.acsnano.org

ARTICLE

Size Controllable, Transparent, and Flexible 2D Silver Meshes Using Recrystallized Ice Crystals as Templates

Shuwang Wu,[†,‡] Linhai Li,[†,‡] Han Xue,[†,‡] Kai Liu,[†,‡] Qingrui Fan,[†,‡] Guoying Bai,[†,‡] and Jianjun Wang*[,†,‡]

[†]Key Laboratory of Green Printing, Institute of Chemistry, Chinese Academy of Sciences, Beijing 100190, PR China
[‡]University of Chinese Academy of Sciences, Beijing 100049, PR China

Supporting Information

ABSTRACT: Ice templates have been widely utilized for the preparation of porous materials due to the obvious advantages, such as environmentally benign and applicable to a wide range of materials. However, it remains a challenge to have controlled pore size as well as dimension of the prepared porous materials with the conventional ice template, since it often employs the kinetically not-stable growing ice crystals as the template. For example, there is no report so far for the preparation of 2D metal meshes with tunable pore size based on the ice template, although facile and eco-friendly prepared metal meshes are highly desirable for wearable electronics. Here, we report the preparation of 2D silver meshes with tunable mesh size employing recrystallized ice crystals as templates. Ice recrystallization is a kinetically stable process; therefore, the grain size of recrystallized ice crystals can be easily tuned, *e.g.*, by adding different salts and changing the annealing temperature. Consequently, the size and line width of silver meshes obtained after freeze-drying can be easily adjusted, which in turn varied the conductivity of the obtained 2D silver film. Moreover, the silver meshes are transparent and display stable conductivity after the repeated stretching and bending. It can be envisioned that this approach for the preparation of 2D conducting films is of practical importance for wearable electronics. Moreover, this study provides a generic approach for the fabrication of 2D meshes with a controllable pore size.

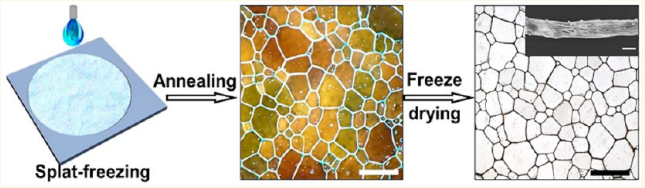

KEYWORDS: *ice recrystallization, size controllable, ice templates, silver meshes, wearable electronics*

Preparation of functional materials with ice as templates has been extensively explored[1−10] and utilized,[11−18] since ice as the template has rich varieties of advantages. First, it can be utilized to template a wide range of materials, such as silicic acid,[1] inorganic salts,[18] polymers,[19] microgel,[20] nanoparticles,[21,22] 2D materials,[23−25] nanowires,[26] *etc.* Second, materials fabricated *via* ice templates have different kinds of structures like aligned pores,[3,27,28] bricks-and-mortar structures,[2] fibers,[20,29,30] colloidal nanoparticles chains[21] and foam.[22] Third, structural materials obtained from ice-template approach can achieve versatile functionalities in various fields such as biomimetic materials,[2,11] cell culturing and separating,[31,32] fire retarding,[14] sensing,[22−24] electrodes[33,34] and so on. Up-to-now, these differently structured materials with various functionalities are prepared by using different freezing methods, *e.g.*, directional freezing,[2] fast freezing[10,29,30] (dripping aqueous solutions into liquid nitrogen) or freeze−thawing.[13,21] These freezing processes are often kinetically not stable,[35] and consequently it is not trivial to tune the structure of the functional materials, although materials with tunable structures are frequently required for practical applications.[4,18] One prominent example is that there is no report on the preparation 2D conducting metal meshes with tunable pore sizes, which is of great importance for wearable electronics.[36−42]

Recently, we have discovered that ions have a profound effect on ice recrystallization which occurs mainly through the process of Ostwald ripening[43] *i.e.*, large ice crystals grow at the expense of small ones, resulting in an increase in the mean crystal size and a decrease in the total number of crystals; and the grain size of recrystallized ice crystals can be easily adjusted by the type of ions in the aqueous solution, the annealing time and temperature.[44] Moreover, our investigation indicated that recrystallized ice crystals could be an alternative ice templates and 2D meshes of polymers and nanoparticles have been prepared. However, nanofibers have not been examined. When fabricating flexible conductors, conductivity and mechanical stability must be considered at the first place and nanofibers such as silver nanowires are ideal candidate materials. In this

Received: May 31, 2017
Accepted: August 24, 2017
Published: August 24, 2017

DOI: 10.1021/acsnano.7b03821
ACS Nano 2017, 11, 9898−9905

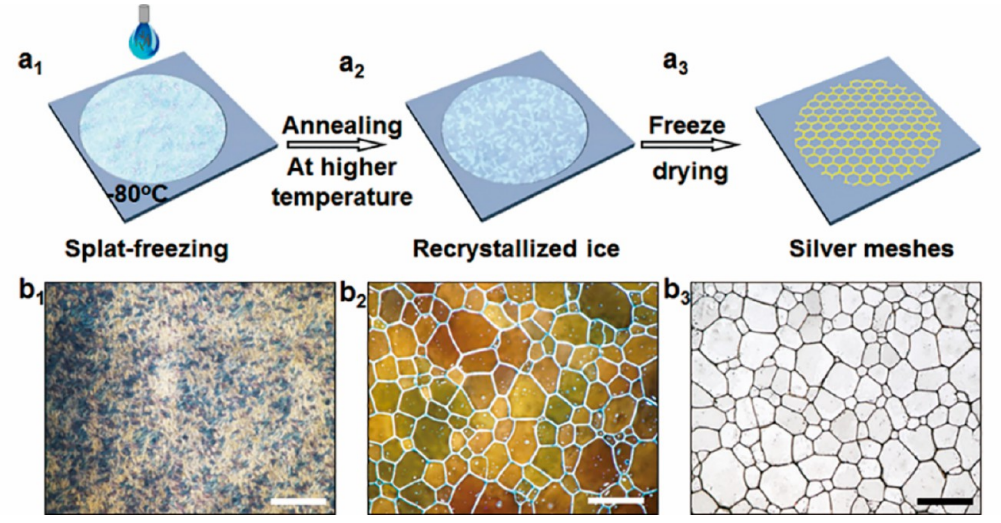

Figure 1. Scheme of the fabrication process of silver meshes using recrystallized ice as the template. (a_1) First, a droplet of silver nanowires suspension was spat-frozen onto the precooled (−80 °C) cover glass. (a_2) Then the frozen sample was annealed for 40 min at a higher temperature, forming the recrystallized ice crystals. (a_3) At last, the sample was freeze-dried and the silver meshes were obtained. (b_1) Polarized optical microscopy (POM) image shows that a large amount of ice crystals formed right after the splat-freezing; (b_2) POM image displays the recrystallized ice after annealing at −5 °C for 40 min and (b_3) POM image reveals the interconnected silver meshes after freeze-drying. All the scale bars are 200 μm.

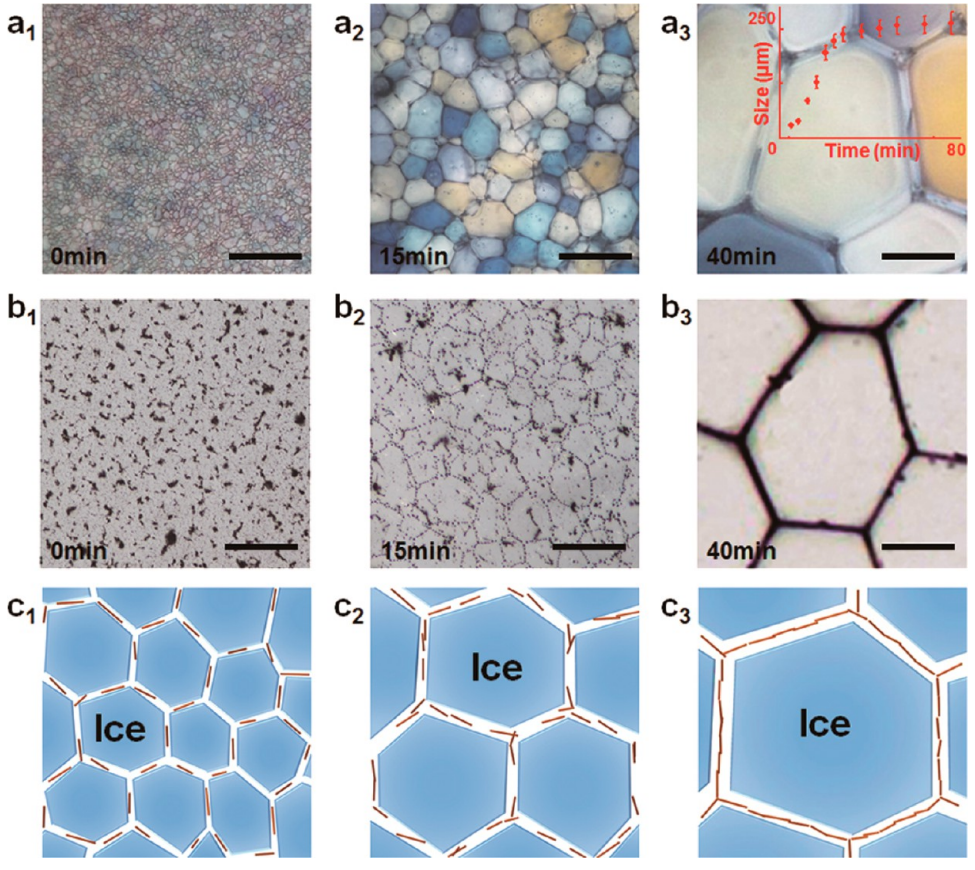

Figure 2. Assembly process of silver nanowires between recrystallized ice crystals reveals the mechanism of the formation of silver meshes. (a) The ice crystals obtained from the silver nanowires dispersion after annealing for (a_1) 0 min, (a_2) 15 min and (a_3) 40 min. The inset shows the evolution of the average size of ice crystals as a function of the annealing time, which indicates that the size of ice crystals levels off after annealed for 40 min. Optical microscopic images show the corresponding locations of silver nanowires; (b_1) the silver nanowires are distributed randomly on the cover glass before annealing. (b_2) Most nanowires are distributed randomly after annealing for 15 min, however, the meshes start to form. (b_3) The meshes are becoming obvious, and interconnected meshes are obtained after annealing for 40 min. And the mechanism is shown as (c_1) without annealing, the silver nanowires of a low concentration are dispersed and trapped between ice crystals, (c_2) after annealing, the size of ice crystals become larger and the number decreases, as such the concentration of the silver nanowire between ice crystals is more concentrated. (c_3) With further annealing, the nanowires are concentrated and become interconnected finally. The polycrystalline ice obtained from 0.2 wt % nanowires with 0.1 mg/mL NaI. All the scale bars are 200 μm.

DOI: 10.1021/acsnano.7b03821
ACS Nano 2017, 11, 9898−9905

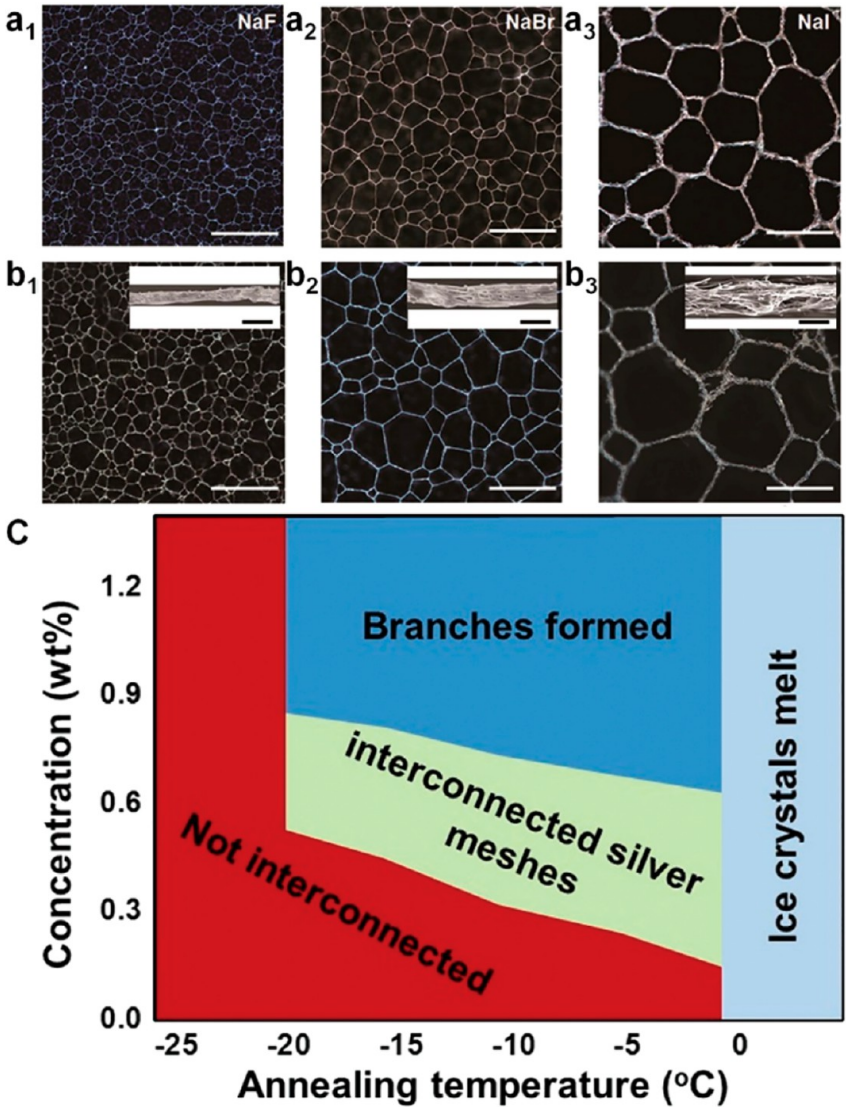

Figure 3. Adjusting sizes of silver meshes by adding different ions and changing annealing temperature. (a_1–a_3) The silver meshes obtained by adding (a_1) NaF, (a_2) NaBr, (a_3) NaI in the aqueous silver nanowire dispersion before freezing (the annealing temperature is −1 °C); and (b_1–b_3) display the silver mesh obtained at annealing temperatures of (b_1) −20 °C, (b_2) −10 °C and (b_3) −1 °C. The concentration of salts and silver nanowires are 0.5 mg/mL and 0.5 wt % respectively. (c) The chart shows the optimal conditions for fabricating sliver meshes. The scale bars, (a) and (b), 200 μm; insets of (b), 2 μm.

study, we fabricate conducting 2D silver meshes by employing the recrystallized ice crystals as templates. We demonstrate that the pore size and line width of silver meshes can be easily tuned by the addition of different ions in the silver nanowire dispersion as well as the annealing temperature during the recrystallization process. This in consequence tunes the conductivity and transparence of the 2D silver mesh. Note that conductive meshes can be directly obtained without further treatments, which benefits from enhanced connectivity between the nanowires. Interestingly the fabricated 2D silver meshes can be easily transferred on the surface of elastomers, and the conductivity is retained after repeated bending and stretching.

RESULTS AND DISCUSSION

The silver nanowires were synthesized with a modified polyol reduction process.[45] The length of the as-prepared silver nanowire is 7.9 ± 1.5 μm and the diameter is ∼30 nm which were measured with SEM and TEM (see Figure S1d–f). Figure S1g shows the X-ray diffraction (XRD) pattern recorded from silver nanowires, with all peaks assigned to be (111), (200), (220), (311) and (222) planes of silver, respectively.[46] At the same time, high-resolution TEM (HRTEM) images (Figure S1h) and the electron diffraction pattern (Figure S1i) reveal that the silver nanowires are highly crystalline.[47] The fabrication process of silver meshes is schematically illustrated in Figure 1a. First a droplet of silver nanowires aqueous dispersion was dripped onto a deeply supercooled (−80 °C) cover glass surface with the vertical distance from the cover glass surface to the nozzle being 1.5 m. Upon impinging on the surface of the cover glass, the droplet spread quickly on the cover glass surface and then froze.[48] As the surface temperature of the cover glass was below the homogeneous ice nucleation temperature[49,50] (Figure 1a_1), ice nucleation occurred spontaneously and consequently a large amount of ice crystals formed. Figure 1b_1 is a typical optical microscopic image of the splat frozen droplets, exhibiting the formed small ice crystals. Then the ice crystals were annealed at a higher temperature (−20, −15, −10, −5, −1 °C, Figure 1a_2), which led to the growth of large crystals with the expense of

DOI: 10.1021/acsnano.7b03821
ACS Nano 2017, 11, 9898–9905

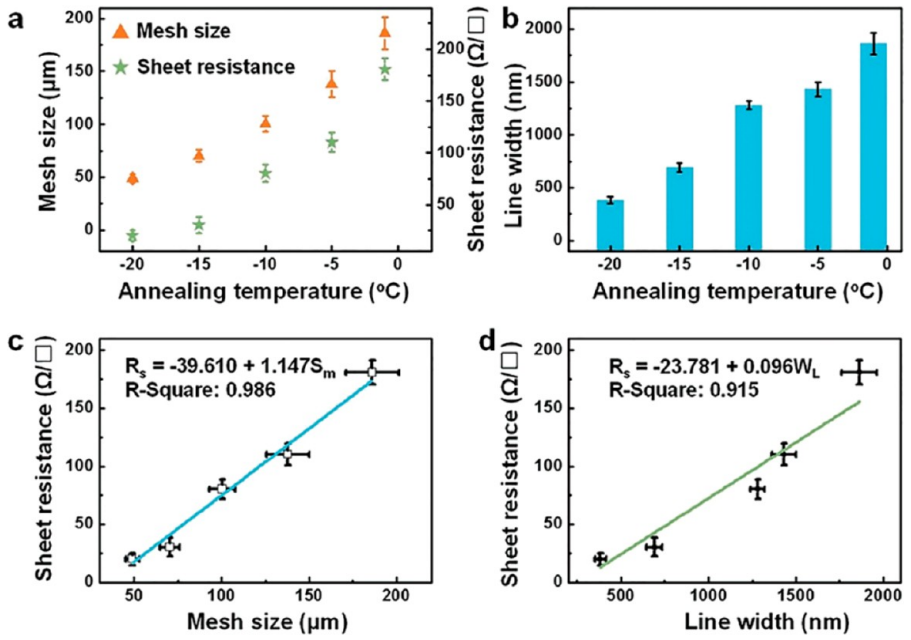

Figure 4. Mesh size, line width and sheet resistance change along with annealing temperature and their relation. (a) The mesh size and the corresponding sheet resistance can be varied by changing the annealing temperature. (b) The line width also varies with the annealing temperature. (c,d) The sheet resistance of flexible electrode varies along with mesh size and line width, respectively. In the equations, R_s: sheet resistance, S_m: mesh size, W_L: line width. Error bars represent the standard deviation.

small ice crystals, *i.e.*, ice recrystallization (Figure S2). And Figure 1b$_2$ verified that after annealing at −5 °C for 40 min the average size of ice crystals increased while the number of ice crystals decreased. Silver meshes were obtained when the recrystallized ice crystals were freeze-dried (Figure 1a$_3$ and b$_3$).

Note that the splat freezing is critical. For comparison, we also immersed a thin film of the silver nanowires dispersion horizontally or vertically into liquid nitrogen (the dispersion was sandwiched between two cover glasses with 10 μm microspheres being the spacer, which is close to the thickness of the ice wafer formed by splat freezing[36−42] (see Figure S3). After annealing and freeze-drying, the silver nanowires immersed into liquid nitrogen horizontally were assembled into pores which were not fully interconnected (Figure S4), and no silver nanowire pores were observed when immersed vertically (Figure S5). These observations can be reconciled when one considers the following facts: at the moments of the droplet impinging on the deeply precooled cover glass, the droplet spreads quickly making the liquid layer being fully contact with the deeply cooled surface (−80 °C). This ensures the efficient heat transfer and thus huge amounts of homogeneous ice nuclei form and grow simultaneously into large ice crystals. At the annealing stage, these ice crystals go through kinetically stable recrystallization. In strong contrast, in the immersing approach the heat transfer is not as efficient as the spat freezing one (thermal conductivity of substrates could not be neglected), and heterogeneous ice nucleation occurs; once the nucleation happens, the latent heat produced cannot be transferred spontaneously and can suppress the occurrence of nucleation in the surrounding. Consequently much less numbers of ice crystals form *via* the kinetically not stable growth process.[3]

To figure out how the silver nanowires were assembled into interconnected meshes during the ice recrystallization process, we followed the assembly process by freeze-drying the recrystallized ice crystals (Figure 2a) and monitor the location of silver nanowires. The structures obtained are shown in Figure 2b. Without annealing (Figure 2b$_1$), the silver nanowires are distributed randomly on cover glass. After annealing for 15 min, most nanowires are distributed randomly, however, the interconnected meshes start to appear (Figure 2b$_2$). With further annealing, the mean size of ice crystals levels off (inset of Figure 2a$_3$) and the meshes are becoming obvious and interconnected meshes are obtained after annealing for 40 min (Figure 2b$_3$). Note that, after the appearance of meshes, as the annealing process going on, the meshes sizes are enlarged and becoming interconnected; at the same time, the width of lines increases. This process is in consistent with the assembling process of fluorescence nanoparticles observed with fluorescence microscope in our previous work.[44] Therefore, we conclude the mechanism of the formation of silver meshes as shown in Figure 2c. When the silver nanowires suspension is splat frozen, many small ice crystals form immediately and the nanowires are dispersed and trapped between ice crystals[51−53] (Figure 2c$_1$); with annealing at a higher temperature, ice recrystallization happens, larger ice crystals grow at the expense of smaller ones (Figure S6), resulting in the substantial decrease of the number of ice crystals, which makes the volume of the silver nanowire dispersion between ice crystals decrease; consequently the silver nanowires become more concentrated, and finally connect with each other forming the interconnected meshes(Figure 2c$_2$ and 2c$_3$).

According to our previous study,[44] there are several factors that determine the ultimate size of ice crystals, such as annealing temperature and time, the type and the concentration of ions/additives. And we investigated systematically the influence of different parameters on the formation of silver meshes (salt concentration, quench temperature, silver nanowire concentration and annealing temperature; see Figure S7−12). Here, the mesh size can be tuned by employing different types of ions (Figure 3a) or changing the annealing temperature (Figure 3b). Figure 3a shows the meshes obtained by adding

DOI: 10.1021/acsnano.7b03821
ACS Nano 2017, 11, 9898−9905

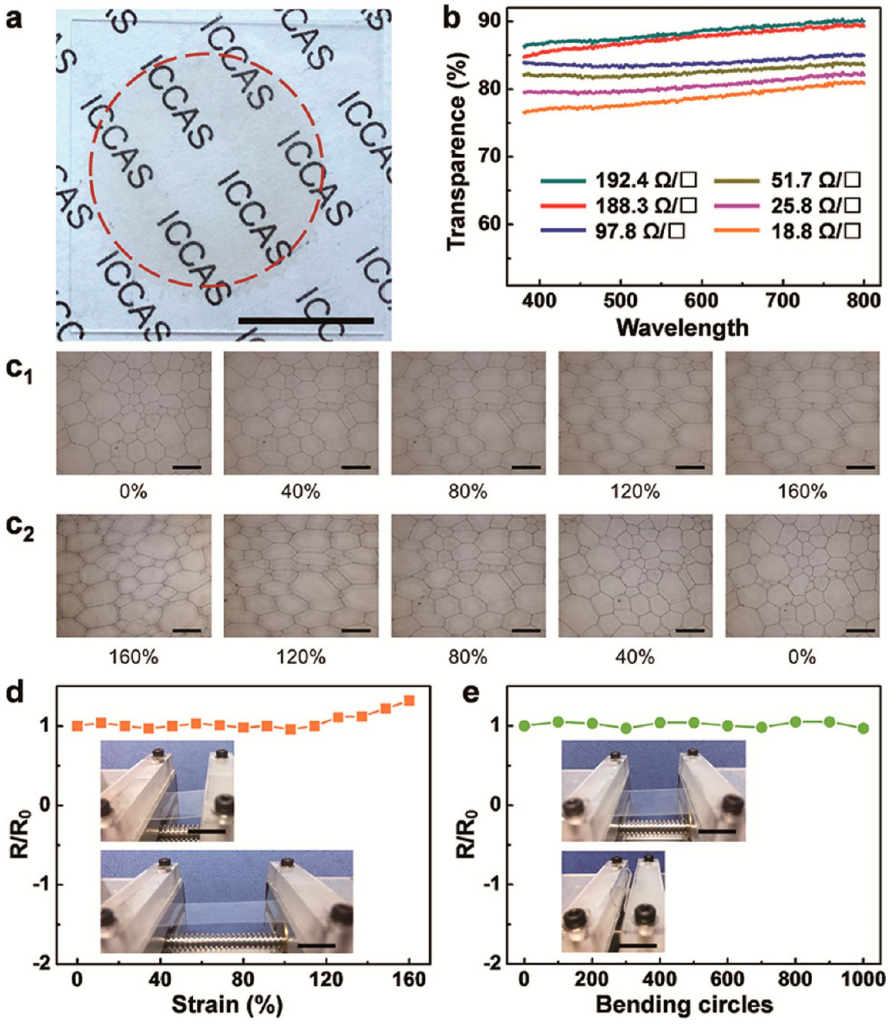

Figure 5. (a) Photograph of the transparent silver meshes on a cover glass surface. (b) Change of the transparency and sheet resistance of the six chosen samples (25.8, 97.8, and 188.3Ω/□ are the sheet resistance of silver meshes obtained from NaF, NaBr and NaI silver nanowire dispersions respectively; meanwhile, 18.8, 51.7, and 192.4 Ω/□ are the sheet resistance of silver meshes obtained from different annealing temperatures, −20, −10, and −1 °C). Deformation (c_1) and recovering (c_2) of silver meshes during stretching. (d) and (e) show the resistance variation during stretching and bending respectively, which indicates the conductivity stability of the as-prepared silver meshes. Scale bars, (a) 1.5 cm, (c) 200 μm, (d,e) 1 cm. ICCAS logo in (a) was used with permission of Institute of Chemistry, Chinese Academy of Sciences.

NaF (Figure 3a$_1$), NaBr (Figure 3a$_2$) and NaI (Figure 3a$_3$). The corresponding sizes are 43.3 ± 3.9 μm, 120.7 ± 5.4 μm and 186.2 ± 32.3 μm. Moreover, we can further regulate the mesh size by changing the annealing temperature while using NaI as the salt because of its widest tunable size window of ice crystals.[44] The size of interconnected meshes can be tuned from 48.9 ± 6.9 μm to 186.2 ± 32.3 μm as the annealing temperature was varied from −20 °C to −1 °C (Figure 3b$_1$, 3b$_2$, 3b$_3$, 4a and Figure S13). As such we obtain a chart showing the optimal conditions to guide the fabrication of well-connected sliver meshes (Figure 3c). These data verify that the size of the silver mesh can be tuned, which demonstrates obviously the key advantage of recrystallized ice crystals as the template for the preparation of porous materials. Meanwhile the corresponding sheet resistance increased from 20.1 ± 5.1 Ω/□ to 180.8 ± 10.4 Ω/□ (Figure 4a). In addition, the line width was tuned from 381.7 ± 31.5 nm to 1862 ± 101 nm (Figure 4b and insets of Figure 3b). We plotted the sheet resistance against the mesh size (Figure 4c) and line width (Figure 4d) respectively. The data were fitted as following: $R_s = -39.610 + 1.147S_m$; $R_s = -23.781 + 0.096W_L$, where R_s is the sheet resistance, S_m is the mesh size, W_L is the line width. For the transparent conducting film, sheet resistance is related to the combination of wire density and compactness, the curvature and width distribution of wire,[54] mesh structural defects, grain boundary scattering and size of nanopores.[55−57] In our case, the sheet resistance increases with the mesh size.

As exhibited in Figure 5a, the as-prepared silver meshes are transparent. UV−vis spectrophotometer and four point probe were used to further characterize the transparence and sheet resistance of the conductive films respectively, and six typical conductive films obtained from different salts and annealing temperatures shown in Figure 3a and b were chosen to present the properties of transparence and conductivity (Figure 5b). The transparence is between ∼78% and ∼88% while the sheet resistances varies from 18.8 to 192.4 Ω/□. Note that the conductive silver meshes can be stretchable and bendable *via* simply transferring onto elastomers such as PDMS as illustrated in Figure S14. Figure 5c shows that during the stretching, the meshes deform (Figure 5c$_1$); after releasing, the meshes can restore reversibly to their initial form (Figure 5c$_2$). Further, the stability of the conductive repeated stretching and bending is

DOI: 10.1021/acsnano.7b03821
ACS Nano 2017, 11, 9898−9905

further tested using the similar method mentioned in the previous study.[39] The resistance of the conductive film changed little when it is stretched to ~120%; as the elongation is larger than 120%, an increase of the resistance can be observed (Figure 5d). At the same time, after bending 1000 times, there is no apparent change of the resistance (Figure 5e). This kind stretchable and bendable conductive films can be ideal candidates for touch screens and wearable electronics.

CONCLUSION

In summary, we reported an approach for fabrication of 2D silver meshes using recrystallized ice as the template. The advantage of this approach is that the mesh size can be tuned since ice recrystallization is a kinetically stable process. We demonstrate here that the mesh size can be tuned from 48.9 ± 6.9 μm to 186.2 ± 32.3 μm and the line width of the mesh can be regulated from 381.7 ± 31.5 nm to 1862 ± 101 nm by changing the annealing temperature and the type of ions in the dispersion. Moreover, the meshes can be transferred onto elastomer surfaces, and the silver mesh shows stable conductivity after repeated stretching and bending.

METHODS

Silver Nanowires Synthesis. $AgNO_3$, NaF, NaBr, NaI and PVP (MW: 55000 g/mol) were purchased from Sigma-Aldrich; PDMS (Sylgard 184) was bought from Dow Corning. The silver nanowires were synthesized with a modified polyol reduction process.[45] Typically, 2.5 g of PVP were added into 180 mL of glycerol in a 500 mL round bottle flask; with tender stirring and heating, PVP was dissolved. After temperature dropped down to room temperature, 0.8 g of silver nitrate was added into the solution. Then a 20 mL of glycerol solution containing 50 mg of NaCl and 0.5 mL of H_2O was added into the flask. The flask was then immersed into a heating mantle equipped with a PTFE paddle stirrer. The reaction flask was then immersed into a heating mantle equipped with a polytetrafluoroethylene (PTFE) paddle stirrer (100 rpm). The solution temperature was raised from room temperature to 180 °C in 20 min. When the temperature reached 180 °C, the heating was stopped. After the temperature cooled to room temperature. Water was added to the solution with 1:1 ratio and the mixture was centrifuged at 8000 rpm. The as-prepared silver nanowires were washed with water three times to remove the PVP residue. After washing, the nanowires suspension was freeze-dried, then dispersed into solution of 0.1, 0.2, 0.3, 0.4, 0.5, 0.6, 0.7, 0.8, 0.9, 1.0, 1.2, 1.5, 2.0 wt %.

Fabrication of Silver Meshes. First a droplet of silver nanowires suspension was splat frozen onto the precooled (−80 °C) cover glass from the height of 1.5 m, forming the polycrystalline ice crystals which are very small. Then the polycrystalline ice crystals were annealed at the higher temperature (−20, −15, −10, −5, −1 °C) for a specific period of time. After annealing, the samples were freeze-dried and the silver meshes were made. To transfer the as-prepared meshes onto PDMS. The precursor of PDMS (PDMS oligomer was mixed with a curing agent, and the ratio is 12.5:1.0) was poured onto the meshes gently, after the precursor leveling, it was heated to 80 °C for 30 min to cross-link. After peeling off the PDMS film carefully, the transparent and flexible film was obtained.

Characterization. All the digital photographs were taken by Nikon eclipse LV 100ND microscope equipped with a CCD (DS-Ri2). SEM images were taken with a JEOL JSM-7500 scanning electron microscope. TEM (JEM-2011) was used to analyze the silver nanowires. When measuring the length silver nanowires, five SEM images were taken randomly and the length was measured with the software of Nano measure 1.2. The XRD spectra was recorded using a Empyrean-2 diffractometer at a scanning rate of 0.05 deg/s. And 2θ ranged from 30° to 90°. The silver nanowires for XRD were drop-casted on cover glass. UV−vis spectrophotometer (UV-9000) and four point probe (ST2558B−F03) were used to characterize the transparence and sheet resistance of the conductive films separately. To test the stability of the conductive film after repeated stretching and bending, conductive silver adhesive (NT-ST60, Nano Top Co., Ltd. China) was pasted on the meshes. Two electrodes were in contacted with two platinum probes to measure the resistance variation on the Keithley 4200-SCS semiconductor analyzer.

ASSOCIATED CONTENT

Supporting Information

The Supporting Information is available free of charge on the ACS Publications website at DOI: 10.1021/acsnano.7b03821.

Figures S1−S14 (PDF)

AUTHOR INFORMATION

Corresponding Author

*E-mail: wangj220@iccas.ac.cn.

ORCID

Jianjun Wang: 0000-0002-1704-9922

Notes

The authors declare no competing financial interest.

ACKNOWLEDGMENTS

The authors thank the financial support from the 973 Program (2013CB933800), the Chinese National Nature Science Foundation (Grant Nos. 51436004, 21421061), and Strategic Priority Research Program of Chinese Academy of Sciences (Grant XDA09020000).

REFERENCES

(1) Mahler, W.; Bechtold, M. F. Freeze-Formed Silica Fibres. *Nature* **1980**, *285*, 27−28.

(2) Deville, S.; Saiz, E.; Nalla, R. K.; Tomsia, A. P. Freezing as a Path to Build Complex Composites. *Science* **2006**, *311*, 515−518.

(3) Zhang, H.; Hussain, I.; Brust, M.; Butler, M. F.; Rannard, S. P.; Cooper, A. I. Aligned Two- and Three-Dimensional Structures by Directional Freezing of Polymers and Nanoparticles. *Nat. Mater.* **2005**, *4*, 787−93.

(4) Bai, H.; Chen, Y.; Delattre, B.; Tomsia, A. P.; Ritchie, R. O. Bioinspired Large-Scale Aligned Porous Materials Assembled with Dual Temperature Gradients. *Sci. Adv.* **2015**, *1*, e1500849.

(5) Deville, S. Ice-templating, Freeze Casting: Beyond Materials Processing. *J. Mater. Res.* **2013**, *28*, 2202−2219.

(6) Deville, S. Understanding the Freezing of Colloidal Suspensions: Crystal Growth and Particle Redistribution. In *Freezing Colloids: Observations, Principles, Control, and Use: Applications in Materials Science, Life Science, Earth Science, Food Science, and Engineering*; Springer International Publishing: Cham, Switzerland, 2017; pp 91−170.

(7) Gutiérrez, M. C.; Ferrer, M. L.; del Monte, F. Ice-Templated Materials: Sophisticated Structures Exhibiting Enhanced Functionalities Obtained after Unidirectional Freezing and Ice-Segregation-Induced Self-Assembly. *Chem. Mater.* **2008**, *20*, 634−648.

(8) Deville, S. Freeze-Casting of Porous Ceramics: A Review of Current Achievements and Issues. *Adv. Eng. Mater.* **2008**, *10*, 155−169.

(9) Deville, S.; Maire, E.; Bernard-Granger, G.; Lasalle, A.; Bogner, A.; Gauthier, C.; Leloup, J.; Guizard, C. Metastable and Unstable Cellular Solidification of Colloidal Suspensions. *Nat. Mater.* **2009**, *8*, 966−972.

(10) Samitsu, S.; Zhang, R.; Peng, X.; Krishnan, M. R.; Fujii, Y.; Ichinose, I. Flash Freezing Route to Mesoporous Polymer Nanofibre Networks. *Nat. Commun.* **2013**, *4*, 2653.

(11) Mao, L. B.; Gao, H. L.; Yao, H. B.; Liu, L.; Cölfen, H.; Liu, G.; Chen, S. M.; Li, S. K.; Yan, Y. X.; Liu, Y. Y.; Yu, S. H. Synthetic Nacre

DOI: 10.1021/acsnano.7b03821
ACS Nano 2017, 11, 9898−9905

by Predesigned Matrix-Directed Mineralization. *Science* **2016**, *354*, 107−110.
(12) Olsson, R. T.; Azizi Samir, M. A. S.; Salazar Alvarez, G.; Belova, L.; Strom, V.; Berglund, L. A.; IkkalaO; NoguesJ; Gedde, U. W. Making Flexible Magnetic Aerogels and Stiff Magnetic Nanopaper Using Cellulose Nanofibrils as Templates. *Nat. Nanotechnol.* **2010**, *5*, 584−588.
(13) Qiu, L.; Liu, J. Z.; Chang, S. L. Y.; Wu, Y.; Li, D. Biomimetic Superelastic Graphene-Based Cellular Monoliths. *Nat. Commun.* **2012**, *3*, 1241.
(14) Wicklein, B.; Kocjan, A.; Salazar-Alvarez, G.; Carosio, F.; Camino, G.; Antonietti, M.; Bergström, L. Thermally Insulating and Fire-Retardant Lightweight Anisotropic Foams Based on Nanocellulose and Graphene Oxide. *Nat. Nanotechnol.* **2015**, *10*, 277−283.
(15) Gao, H. L.; Xu, L.; Long, F.; Pan, Z.; Du, Y. X.; Lu, Y.; Ge, J.; Yu, S. H. Macroscopic Free-Standing Hierarchical 3D architectures Assembled From Silver Nanowires by Ice Templating. *Angew. Chem., Int. Ed.* **2014**, *53*, 4561−6.
(16) Gutierrez, M. C.; Ferrer, M. L.; Yuste, L.; Rojo, F.; del Monte, F. Bacteria Incorporation in Deep-Eutectic Solvents through Freeze-Drying. *Angew. Chem., Int. Ed.* **2010**, *49*, 2158−2162.
(17) Guo, T.; Che, P.; Heng, L.; Fan, L.; Jiang, L. Anisotropic Slippery Surfaces: Electric-Driven Smart Control of a Drop's Slide. *Adv. Mater.* **2016**, *28*, 6999−7007.
(18) Bai, H.; Walsh, F.; Gludovatz, B.; Delattre, B.; Huang, C.; Chen, Y.; Tomsia, A. P.; Ritchie, R. O. Bioinspired Hydroxyapatite/Poly(methyl methacrylate) Composite with a Nacre-Mimetic Architecture by a Bidirectional Freezing Method. *Adv. Mater.* **2016**, *28*, 50−56.
(19) Landi, E.; Valentini, F.; Tampieri, A. Porous Hydroxyapatite/Gelatine Scaffolds with Ice-Designed Channel-Like Porosity for Biomedical Applications. *Acta Biomater.* **2008**, *4*, 1620−1626.
(20) Shi, Q.; An, Z.; Tsung, C. K.; Liang, H.; Zheng, N.; Hawker, C. J.; Stucky, G. D. Ice-Templating of Core/Shell Microgel Fibers through 'Bricks-and-Mortar' Assembly. *Adv. Mater.* **2007**, *19*, 4539−4543.
(21) Shen, X.; Chen, L.; Li, D.; Zhu, L.; Wang, H.; Liu, C.; Wang, Y.; Xiong, Q.; Chen, H. Assembly of Colloidal Nanoparticles Directed by the Microstructures of Polycrystalline Ice. *ACS Nano* **2011**, *5*, 8426−8433.
(22) Colard, C. A. L.; Cave, R. A.; Grossiord, N.; Covington, J. A.; Bon, S. A. F. Conducting Nanocomposite Polymer Foams from Ice-Crystal-Templated Assembly of Mixtures of Colloids. *Adv. Mater.* **2009**, *21*, 2894−2898.
(23) Sun, H.; Xu, Z.; Gao, C. Multifunctional, Ultra-Flyweight, Synergistically Assembled Carbon Aerogels. *Adv. Mater.* **2013**, *25*, 2554−2560.
(24) Estevez, L.; Kelarakis, A.; Gong, Q.; Da'as, E. H.; Giannelis, E. P. Multifunctional Graphene/Platinum/Nafion Hybrids via Ice Templating. *J. Am. Chem. Soc.* **2011**, *133*, 6122−6125.
(25) Zeng, X.; Ye, L.; Yu, S.; Sun, R.; Xu, J.; Wong, C. P. Facile Preparation of Superelastic and Ultralow Dielectric Boron Nitride Nanosheet Aerogels via Freeze-Casting Process. *Chem. Mater.* **2015**, *27*, 5849−5855.
(26) Ferraro, C.; Garcia-Tuñon, E.; Rocha, V. G.; Barg, S.; Fariñas, M. D.; Alvarez-Arenas, T. E. G.; Sernicola, G.; Giuliani, F.; Saiz, E. Light and Strong SiC Networks. *Adv. Funct. Mater.* **2016**, *26*, 1636−1645.
(27) Nishihara, H.; Mukai, S. R.; Yamashita, D.; Tamon, H. Ordered Macroporous Silica by Ice Templating. *Chem. Mater.* **2005**, *17*, 683−689.
(28) Zhang, H.; Cooper, A. I. Aligned Porous Structures by Directional Freezing. *Adv. Mater.* **2007**, *19*, 1529−1533.
(29) Zhang, H.; Lee, J. Y.; Ahmed, A.; Hussain, I.; Cooper, A. I. Freeze-Align and Heat-Fuse: Microwires and Networks from Nanoparticle Suspensions. *Angew. Chem., Int. Ed.* **2008**, *47*, 4573−4576.
(30) Xu, Z.; Zhang, Y.; Li, P.; Gao, C. Strong, Conductive, Lightweight, Neat Graphene Aerogel Fibers with Aligned Pores. *ACS Nano* **2012**, *6*, 7103−7113.
(31) O'Brien, F. J.; Harley, B. A.; Yannas, I. V.; Gibson, L. J. The Effect of Pore Size on Cell Adhesion in Collagen-GAG Scaffolds. *Biomaterials* **2005**, *26*, 433−441.
(32) Murphy, C. M.; Haugh, M. G.; O'Brien, F. J. The Effect of Mean Pore Size on Cell Attachment, Proliferation and Migration in Collagen−Glycosaminoglycan Scaffolds for Bone Tissue Engineering. *Biomaterials* **2010**, *31*, 461−466.
(33) Hu, Y.; Luo, B.; Ye, D.; Zhu, X.; Lyu, M.; Wang, L. An Innovative Freeze-Dried Reduced Graphene Oxide Supported SnS_2 Cathode Active Material for Aluminum-Ion Batteries. *Adv. Mater.* **2017**, 1606132.
(34) Shao, Y.; El-Kady, M. F.; Lin, C. W.; Zhu, G.; Marsh, K. L.; Hwang, J. Y.; Zhang, Q.; Li, Y.; Wang, H.; Kaner, R. B. 3D Freeze-Casting of Cellular Graphene Films for Ultrahigh-Power-Density Supercapacitors. *Adv. Mater.* **2016**, *28*, 6719−6726.
(35) Balluffi, R. W.; Allen, S.; Carter, W. C. *Kinetics of Materials*; John Wiley & Sons, 2005.
(36) Layani, M.; Gruchko, M.; Milo, O.; Balberg, I.; Azulay, D.; Magdassi, S. Transparent Conductive Coatings by Printing Coffee Ring Arrays Obtained at Room Temperature. *ACS Nano* **2009**, *3*, 3537−3542.
(37) Huang, Z.; Su, M.; Yang, Q.; Li, Z.; Chen, S.; Li, Y.; Zhou, X.; Li, F.; Song, Y. A General Patterning Approach by Manipulating the Evolution of Two-Dimensional Liquid Foams. *Nat. Commun.* **2017**, *8*, 14110.
(38) Han, B.; Huang, Y.; Li, R.; Peng, Q.; Luo, J.; Pei, K.; Herczynski, A.; Kempa, K.; Ren, Z.; Gao, J. Bio-Inspired Networks for Optoelectronic Applications. *Nat. Commun.* **2014**, *5*, 5674.
(39) Jiang, J.; Bao, B.; Li, M.; Sun, J.; Zhang, C.; Li, Y.; Li, F.; Yao, X.; Song, Y. Fabrication of Transparent Multilayer Circuits by Inkjet Printing. *Adv. Mater.* **2016**, *28*, 1420−1426.
(40) Zeng, Z.; Huang, X.; Yin, Z.; Li, H.; Chen, Y.; Li, H.; Zhang, Q.; Ma, J.; Boey, F.; Zhang, H. Fabrication of Graphene Nanomesh by Using an Anodic Aluminum Oxide Membrane as a Template. *Adv. Mater.* **2012**, *24*, 4138−4142.
(41) Rao, K. D. M.; Gupta, R.; Kulkarni, G. U. Fabrication of Large Area, High-Performance, Transparent Conducting Electrodes Using a Spontaneously Formed Crackle Network as Template. *Adv. Mater. Interfaces* **2014**, *1*, 1400090.
(42) Suh, Y. D.; Kwon, J.; Lee, J.; Lee, H.; Jeong, S.; Kim, D.; Cho, H.; Yeo, J.; Ko, S. H. Maskless Fabrication of Highly Robust, Flexible Transparent Cu Conductor by Random Crack Network Assisted Cu Nanoparticle Patterning and Laser Sintering. *Adv. Electro. Mater.* **2016**, *2*, 1600277.
(43) Voorhees, P. W. The theory of Ostwald ripening. *J. Stat. Phys.* **1985**, *38*, 231−252.
(44) Wu, S.; Zhu, C.; He, Z.; Xue, H.; Fan, Q.; Song, Y.; Francisco, J. S.; Zeng, X. C.; Wang, J. Ion-Specific Ice Recrystallization Provides a Facile Approach for the Fabrication of Porous Materials. *Nat. Commun.* **2017**, *8*, 15154.
(45) Yang, C.; Gu, H.; Lin, W.; Yuen, M. M.; Wong, C. P.; Xiong, M.; Gao, B. Silver Nanowires: From Scalable Synthesis to Recyclable Foldable Electronics. *Adv. Mater.* **2011**, *23*, 3052−3056.
(46) Sun, Y.; Gates, B.; Mayers, B.; Xia, Y. Crystalline Silver Nanowires by Soft Solution Processing. *Nano Lett.* **2002**, *2*, 165−168.
(47) Yang, C.; Gu, H.; Lin, W.; Yuen, M. M.; Wong, C. P.; Xiong, M.; Gao, B. Silver Nanowires: From Scalable Synthesis to Recyclable Foldable Electronics. *Adv. Mater.* **2011**, *23*, 3052−3056.
(48) Knight, C. A.; Hallett, J.; DeVries, A. L. Solute Effects on Ice Recrystallization: An Assessment Technique. *Cryobiology* **1988**, *25*, 55−60.
(49) Sellberg, J. A.; Huang, C.; McQueen, T. A.; Loh, N. D.; Laksmono, H.; Schlesinger, D.; Sierra, R. G.; Nordlund, D.; Hampton, C. Y.; Starodub, D.; et al. Ultrafast X-ray Probing of Water Structure Below the Homogeneous Ice Nucleation Temperature. *Nature* **2014**, *510*, 381−384.
(50) Koop, T.; Luo, B.; Tsias, A.; Peter, T. Water Activity as the Determinant for Homogeneous Ice Nucleation in Aqueous Solutions. *Nature* **2000**, *406*, 611−614.

DOI: 10.1021/acsnano.7b03821
ACS Nano 2017, 11, 9898−9905

(51) Menger, F. M.; Galloway, A. L.; Chlebowski, M. E.; Apkarian, R. P. Ultrastructure in Frozen/Etched Saline Solutions: On The Internal Cleansing of Ice. *J. Am. Chem. Soc.* **2004**, *126*, 5987−5989.
(52) Cheng, J.; Soetjipto, C.; Hoffmann, M. R.; Colussi, A. Confocal Fluorescence Microscopy of the Morphology and Composition of Interstitial Fluids in Freezing Electrolyte Solutions. *J. Phys. Chem. Lett.* **2009**, *1*, 374−378.
(53) Krausko, J.; Runštuk, J.; Neděla, V.; Klán, P.; Heger, D. Observation of a Brine Layer on an Ice Surface with an Environmental Scanning Electron Microscope at Higher Pressures and Temperatures. *Langmuir* **2014**, *30*, 5441−5447.
(54) Kumar, A.; Kulkarni, G. U. Evaluating Conducting Network Based Transparent Electrodes from Geometrical Considerations. *J. Appl. Phys.* **2016**, *119*, 015102.
(55) Maurer, J. H.; González-García, L.; Reiser, B.; Kanelidis, I.; Kraus, T. Templated Self-Assembly of Ultrathin Gold Nanowires by Nanoimprinting for Transparent Flexible Electronics. *Nano Lett.* **2016**, *16*, 2921−2925.
(56) Van De Groep, J.; Spinelli, P.; Polman, A. Transparent Conducting Silver Nanowire Networks. *Nano Lett.* **2012**, *12*, 3138−3144.
(57) Suh, Y. D.; Hong, S.; Lee, J.; Lee, H.; Jung, S.; Kwon, J.; Hyunjin, M.; Phillip, W.; Jaeho, S.; Junyeob, Y.; Ko, S. H.Random Nanocrack, Assisted Metal Nanowire-Bundled Network Fabrication for a Highly Flexible and Transparent Conductor. *RSC Adv.* **2016**, *6*, 57434−57440.

DOI: 10.1021/acsnano.7b03821
ACS Nano 2017, 11, 9898−9905